Zinc activation of OTOP proton channels identifies structural elements of the gating apparatus

Bochuan Teng[1,2†], Joshua P Kaplan[1,2†], Ziyu Liang[1,2], Kevin Saejin Chyung[1], Marcel P Goldschen-Ohm[3], Emily R Liman[1,2*]

[1]Section of Neurobiology, Department of Biological Sciences, University of Southern California, Los Angeles, United States; [2]Program in Neuroscience, University of Southern California, Los Angeles, United States; [3]University of Texas at Austin, Department of Neuroscience, Austin, United States

Abstract Otopetrin proteins (OTOPs) form proton-selective ion channels that are expressed in diverse cell types where they mediate detection of acids or regulation of pH. In vertebrates there are three family members: OTOP1 is required for formation of otoconia in the vestibular system and it forms the receptor for sour taste, while the functions of OTOP2 and OTOP3 are not yet known. Importantly, the gating mechanisms of any of the OTOP channels are not well understood. Here, we show that zinc (Zn^{2+}), as well as other transition metals including copper (Cu^{2+}), potently activates murine OTOP3 (mOTOP3). Zn^{2+} pre-exposure increases the magnitude of mOTOP3 currents to a subsequent acid stimulus by as much as 10-fold. In contrast, mOTOP2 currents are insensitive to activation by Zn^{2+}. Swapping the extracellular tm 11–12 linker between mOTOP3 and mOTOP2 was sufficient to eliminate Zn^{2+} activation of mOTOP3 and confer Zn^{2+} activation on mOTOP2. Mutation to alanine of H531 and E535 within the tm 11–12 linker and H234 and E238 within the 5–6 linker reduced or eliminated activation of mOTOP3 by Zn^{2+}, indicating that these residues likely contribute to the Zn^{2+} activating site. Kinetic modeling of the data is consistent with Zn^{2+} stabilizing the opn2+en state of the channel, competing with H^+ for activation of the channels. These results establish the tm 11–12 and tm 5–6 linkers as part of the gating apparatus of OTOP channels and a target for drug discovery. Zn^{2+} is an essential micronutrient and its activation of OTOP channels will undoubtedly have important physiological sequelae.

*For correspondence: liman@usc.edu

†These authors contributed equally to this work

Editor's evaluation

This valuable study discovers that zinc ions can activate some OTOP proton channels, identifying a pharmacological tool for research, and further establishing that OTOP channels gate. The data presented provides convincing support for conclusions. This work is expected to be of great interest to physiologists studying OTOP channels and other proton-permeation pathways.

Introduction

Pharmacological agents that can activate or inhibit ion channels have long been used as probes to describe the fundamental processes of channel gating and ion permeation (*Hille, 2001*). For example, the discovery of the charged molecule TEA and the scorpion toxin charybdotoxin as a specific blocker of K^+ channels allowed for the early identification of residues lining the channel pore well before the channel structures were determined (*MacKinnon et al., 1990*; *Yellen et al., 1991*; *Banerjee et al., 2013*). Similarly, gating modifiers have been used to probe structural rearrangements that

accompany the opening of voltage-gated ion channels (*Swartz and MacKinnon, 1997*; *Sack and Aldrich, 2006*; *Catterall et al., 2007*; *Goldschen-Ohm and Chanda, 2014*). More recently, toxins that target pain-sensing ASIC and TRPV1 channels have been used to probe the conformational states of these channels (*Bohlen et al., 2010*; *Baconguis et al., 2014*). One of the most common modulators of channel activity is the trace metal zinc (Zn^{2+}), which can affect gating, permeation, or both (*Gilly and Armstrong, 1982*; *Chu et al., 2004*; *Noh et al., 2015*; *Peralta and Huidobro-Toro, 2016*). Zn^{2+} binds to proteins with high affinity and specificity and regulates a wide range of cellular processes, including metabolism and gene expression (*Vallee and Falchuk, 1993*). Zn^{2+} is a potent inhibitor of proton transport molecules including the voltage-gated proton channel Hv1 and the proton-selective ion channel OTOP1 (*Decoursey, 2003*; *Ramsey et al., 2006*; *Bushman et al., 2015*; *Tu et al., 2018*; *Teng et al., 2019*).

OTOP1 is a member of a family of proteins (*Hughes et al., 2008*; *Hurle et al., 2011*), which includes, within vertebrates, two other members, OTOP2 and OTOP3, that also function as proton channels (*Tu et al., 2018*). OTOP proton channels are expressed throughout the body, where they play diverse and still poorly understood roles in pH sensing and homeostasis. In vertebrates and invertebrates, OTOP channels expressed in the gustatory system sense acids and function as sour taste receptors (OTOP1 for vertebrates; OTOPL1 for *Drosophila*) (*Teng et al., 2019*; *Zhang et al., 2019*; *Ganguly et al., 2021*; *Mi et al., 2021*). In mice and zebrafish, OTOP1 plays an essential role in the formation of force-sensing calcium carbonate-based otoconia in the ear (*Hurle et al., 2003*; *Hughes et al., 2004*), likely by regulating pH in the endolymph. OTOP2 and OTOP3 are both found throughout the digestive system, and their expression has been shown to correlate with disease progression in some forms of colon cancer (*Tu et al., 2018*; *Parikh et al., 2019*; *Yang et al., 2019*). Most recently, an OTOP channel was shown to be critically involved in calcification and the formation of a skeleton in sea urchin embryos (*Chang et al., 2021*).

Given the recent discovery of OTOP proteins as forming ion channels (*Tu et al., 2018*), much remains to be discovered about how they function. For example, it was not known if the channels occupy open and closed states or if those terms even apply to these proteins, which bear no structural similarity to other ion channels, and that could conduct protons through a non-aqueous pathway (*Decoursey, 2003*). Recently, we showed that OTOP channels are gated by extracellular protons, acting mostly likely on multiple titratable residues on the extracellular domain of the protein (*Teng et al., 2022*). Here, we report the first evidence that OTOP channels can be activated by Zn^{2+} and Cu^{2+}. This confirms that OTOP channels are gated, like nearly all other ion channels. Using a chimeric channel approach and point mutations, we identify residues in the linkers between tm 11-12 and tm 5-6 that represent key determinants for and likely form the Zn^{2+} activating site. We further propose that the elements of the gating apparatus of the channels that we identify are potential targets for pharmacological manipulation.

Results

Zn^{2+} both blocks and potentiates OTOP3 currents

While measuring the sensitivity of the three murine OTOP channels to inhibition by Zn^{2+}, we noticed that mOTOP3 currents were larger following removal of Zn^{2+} than before its introduction. We refer to this activating effect of Zn^{2+} as potentiation. For these and other experiments, murine OTOP channels were expressed in HEK-293 cells and studied by patch-clamp recording. As shown in *Figure 1*, all three murine OTOP channels carried inward currents in response to a pH 5.5 stimulus and were subsequently inhibited by 1 mM Zn^{2+} at pH 5.5. However, only mOTOP3 currents showed recovery during the Zn^{2+} exposure and a large rebound, of nearly threefold, following its removal (*Figure 1A and B*). The potentiating effect of Zn^{2+} was dose-dependent over a concentration range of 0.1–10 mM and did not show evidence of saturation (*Figure 1C and D*). This contrasts with the inhibitory effect of Zn^{2+} on mOTOP3 currents, which for a stimulus of pH 5.5 showed clear saturation at 3 mM and could be fit with an $IC_{50}=0.31$ mM (*Figure 1D*). The difference in the dose dependence of inhibition and potentiation suggests that Zn^{2+} interacts with distinct binding sites on the channels to produce the two effects (see below).

We next asked whether the effect of Zn^{2+} to potentiate the mOTOP3 currents was through actions on the extracellular or the intracellular side of the channel, possibly following entry into the cytosol as
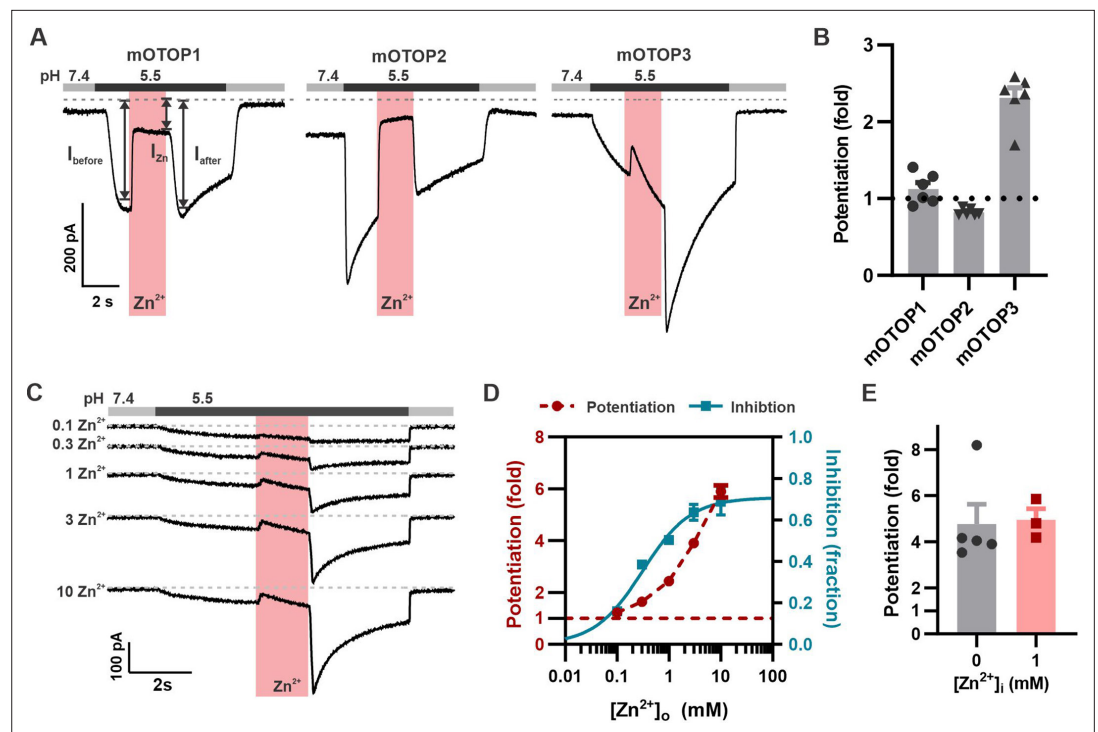
Figure 1. Zn^{2+} blocks and potentiates mOTOP3 currents. (**A**) Representative traces show Zn^{2+} both inhibits and potentiates mOTOP3 currents. Proton currents were elicited in HEK293 cells expressing each of the three mOTOP channels in response to lowering the extracellular pH to 5.5 in the absence of extracellular Na^+ as indicated. Zn^{2+} (pink bar, 1 mM) inhibits currents through all three channels, but only mOTOP3 currents are potentiated following Zn^{2+} removal. V_m was held at –80 mV. (**B**) Average and all points data for experiments as in (**A**) showing fold potentiation as measured by comparing the current magnitude before and after Zn^{2+} application (arrows shown in **A**) .(**C**) Zn^{2+} applied at varying concentrations (pink bar, concentration indicated in mM) produces a dose-dependent inhibition and potentiation of mOTOP3 currents. (**D**) Average data from experiments in (C) show the dose dependence of potentiation and inhibition (n=4 for Zn^{2+} potentiation, n=6 for Zn^{2+} inhibition). The dose dependence of Zn^{2+} inhibition was fit with a Hill equation, with an IC_{50}=0.31 mM, and Hill coefficient = 0.94. (**E**) Average potentiation of mOTOP3 currents in response to 1 mM extracellular Zn^{2+} with (gray) or without (pink) 1 mM Zn^{2+} loaded in the pipette. There was no difference between the two conditions (Student's t-test, p=0.88).

The online version of this article includes the following source data for figure 1:

Source data 1. Source data for **Figure 1**.

is the case for TRPA1 (**Hu et al., 2009**). Introducing 1 mM Zn^{2+} into the patch pipette did not change the degree of potentiation in response to 1 mM extracellular Zn^{2+}, indicating that Zn^{2+} likely acts on extracellular domains of the channel (**Figure 1E**).

Pre-exposure to Zn²⁺ potentiates OTOP3 currents

To study the activating effects of Zn^{2+} on mOTOP3 and avoid confounds due to its inhibitory effect, we devised a recording protocol in which the cells were pre-exposed to Zn^{2+} at pH 7.4, prior to evoking currents with an acidic stimulus (pH 5.5). As shown in **Figure 2A**, this produced a robust potentiation of mOTOP3 currents evoked in response to the pH 5.5 stimulus. Notably, the currents were both faster and larger after exposure to Zn^{2+}.

We measured the dose and time dependence of potentiation by Zn^{2+}, using three concentrations of Zn^{2+}: 0.3, 1, and 3 mM and by varying the duration of the Zn^{2+} pre-exposure from 1 to 64 s. The response to Zn^{2+} was compared to the response in the absence of Zn^{2+} from the same cell. As shown in **Figure 2B and C**, 3 mM Zn^{2+} caused a more than 10-fold increase in the peak current, the lowest concentration of Zn^{2+}, 0.3 mM, applied for up to 64 s produced only a negligible increase in the peak current and 1 mM Zn^{2+} had an intermediate effect. Thus, the potentiating effect of Zn^{2+}, as measured by the peak current, was dose-dependent, with an apparent threshold of >0.3 mM Zn^{2+}. Examination
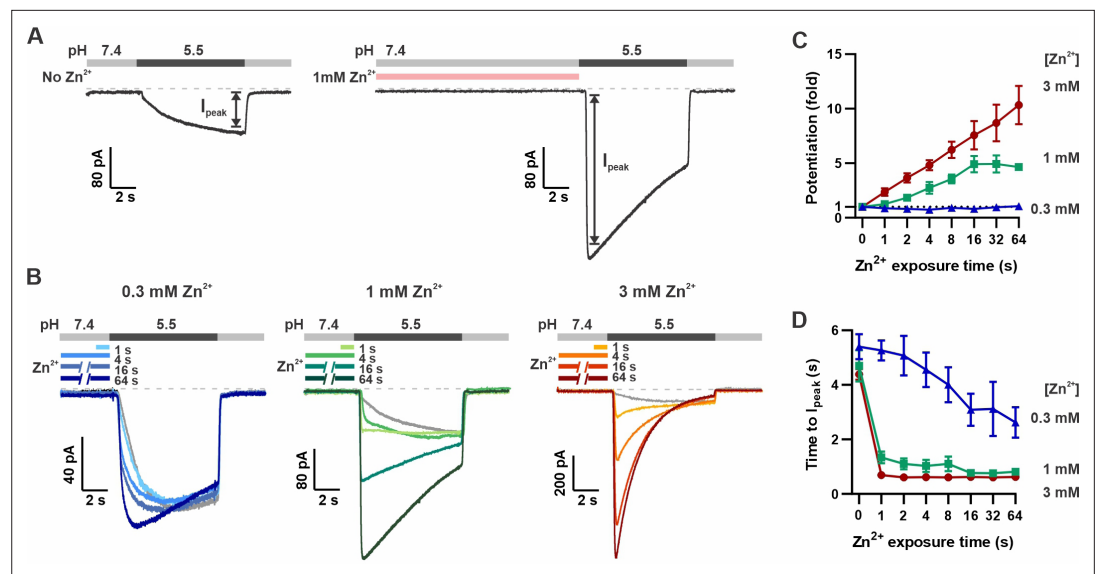
Figure 2. Pre-exposure to Zn^{2+} potentiates mOTOP3 currents in a dose- and time-dependent manner. (**A**) Solution exchange protocol designed to measure effects of Zn^{2+} on gating of OTOP currents without confounds due to its inhibitory effects. V_m was held at –80 mV. In this example, currents were elicited to a pH 5.5 stimulus without pre-exposure to Zn^{2+} and then following a 16 s exposure to 1 mM Zn^{2+}. (**B**) Representative traces show mOTOP3 currents elicited in response to pH 5.5 stimulus with pre-exposure to 0.3 mM (blue), 1 mM (green), and 3 mM (orange/red) Zn^{2+} for durations from 1 to 64 s as indicated. (**C, D**) The fold potentiation (**C**) and time to I_{peak} (**D**) as a function of Zn^{2+} pre-exposure time from experiments as in (B) (n=5–7). Fold potentiation was measured as the ratio of the current evoked to the pH 5.5 stimulus after Zn^{2+} to the control response in the absence of Zn^{2+}. Data are plotted as mean ± s.e.m.

The online version of this article includes the following source data for figure 2:

Source data 1. Source data for *Figure 2*.

of the time dependence of the response showed increasing potentiation with exposure times up to ~16 s for concentrations of 1 and 3 mM Zn^{2+}, at which point the effect tended to saturate, although there was some variability from cell to cell (*Figure 2C*).

In addition to increasing the peak current, Zn^{2+} pre-exposure also increased the apparent rate of activation to a pH 5.5 stimulus that otherwise slowly activates mOTOP3 currents (*Teng et al., 2022*). This change in apparent activation kinetics showed a dose and time dependence (*Figure 2D*). At the higher concentrations (1 and 3 mM), an exposure of 1 s was sufficient to observe a maximal decrease in the time to peak current from ~4 s to <1 s. At 0.3 mM Zn^{2+}, this effect required longer exposure times, and activation rates never reached the speed obtained with 1 s exposure to 1 mM Zn^{2+}. To assess the stability of the Zn^{2+} bound conformation, we measured the rate of recovery from potentiation by Zn^{2+} (*Figure 3*). For these experiments, the cells were exposed to 1 mM Zn^{2+} (pH 7.4) for 16 s. This was followed by a 'wash-off' period of 0–64 s in a Zn^{2+}-free solution (pH 7.4) before currents were activated with a pH 5.5 solution (*Figure 3A*). A wash-off period of 1 s was sufficient to reduce potentiation by 50% while a period of >16 s allowed for a complete recovery of currents to baseline.

Thus, application of millimolar concentrations of Zn^{2+} at pH 7.4 elicits upon its removal a robust concentration- and time-dependent potentiation of mOTOP3 currents.

OTOP1 is mildly potentiated by Zn^{2+}

Using this new protocol, we went back and assessed the effect of Zn^{2+} on mOTOP1 and mOTOP2. mOTOP1 and mOTOP2 currents evoked in response to a solution at pH 5.5 showed little to no evidence of potentiation by exposure to 1 mM Zn^{2+} applied for 16 s at pH 7.4 (*Figure 4A and B*). As mOTOP1 and mOTOP2 differ from mOTOP3 channels in that they display a greater degree of activation at pH 5.5 (*Teng et al., 2022*), we considered whether this might preclude further potentiation by Zn^{2+}. Indeed, we found that mOTOP1 currents evoked in response to a pH 6.0 stimulus could be potentiated by as much as threefold after a 64 s exposure to 1 mM Zn^{2+} (*Figure 4C*), with a time
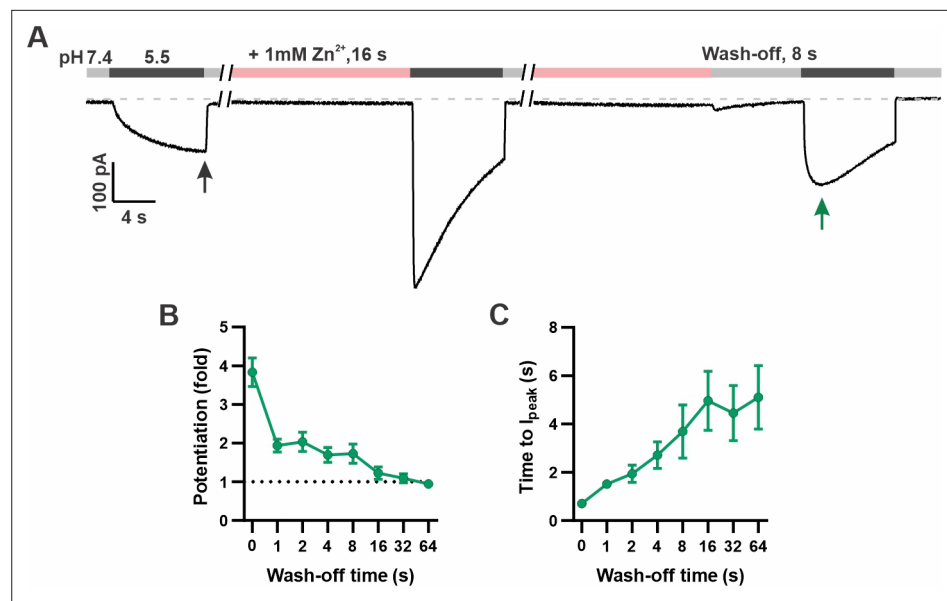
Figure 3. Time dependence of the recovery of mOTOP3 currents from Zn^{2+} pre-potentiation. (**A**) Solution exchange protocol designed to measure the recovery of mOTOP3 currents following exposure to Zn^{2+}. In this example, the cell expressing mOTOP3 was first exposed to 1 mM Zn^{2+} for 16 s which was followed by an 8 s wash-off phase in pH 7.4 solution before currents were elicited in response to the pH 5.5 solution. (**B, C**) The fold potentiation (**B**) and time to I_{peak} (**C**) as a function of Zn^{2+} wash-off time from experiments as in (**A**) (n=4–6). Data are plotted as mean ± s.e.m.

The online version of this article includes the following source data for figure 3:

Source data 1. Source data for **Figure 3**.

dependence similar to what we observed for mOTOP3 (**Figure 4D**). Activation rates of the more rapidly activating OTOP1 channels were not measurably enhanced by pre-exposure to Zn^{2+} exposure (**Figure 4E**). Thus, potentiation by Zn^{2+} is a feature shared by mOTOP1 and mOTOP3.

Divalent transition metal ions potentiate and block OTOP3

Zn^{2+} modulates gating of a wide range of ion channels and neurotransmitter receptors, some of which are sensitive to other divalent transition metals interacting with the same residues as Zn^{2+} (**Mathie et al., 2006**; **Shcheglovitov et al., 2012**). For example, the zinc-activated ion channel, a member of the family of Cys-loop receptors, is also activated by copper (Cu^{2+}) (**Trattnig et al., 2016**) while the cyclic nucleotide-gated ion channel from rods is potentiated by nickel (Ni^{2+}), cadmium (Cd^{2+}) and cobalt (Co^{2+}), as well as by Zn^{2+}, acting through a histidine residue in the mouth of the channel (**Karpen et al., 1993**; **Gordon and Zagotta, 1995a**). Divalent transition metals such as Co^{2+}, Ni^{2+}, Cu^{2+}, and Cd^{2+} are predicted to have distinct preferred coordination geometries in metalloproteins and other proteins to which they bind but are often coordinated by the same acidic and/or polar residues including histidine, glutamic acid, aspartic acid, and cysteine (**Rulíšek and Vondrášek, 1998**). To gain insights into the nature of the Zn^{2+} binding site, we tested whether other transition metals could potentiate mOTOP3 currents. Each metal ion was presented at a concentration of 1 mM for 16 s prior to activation of currents with a pH 5.5 stimulus. Pre-exposure to Cu^{2+} caused a dramatic increase in the magnitudes of the currents, potentiating them by 11.6±0.1-fold (n=10). Pre-exposure to Cd^{2+} and Ni^{2+} had more modest effects, potentiating mOTOP3 currents by 1.7±0.1 (n=10) and 1.6-fold±0.0 (n=8). In contrast, Co^{2+} and iron (Fe^{2+}) had little to no effect on the magnitude or kinetics of the currents (**Figure 5**). These results suggest that the binding site occupied by Zn^{2+} may also be shared by other d-block transition metals.

We also tested if the metals that activate also inhibit mOTOP3, like Zn^{2+}. Following activation of mOTOP3 by a pH 5.5 stimulus, and in the continued presence of the stimulus, each metal was applied at a concentration of 1 mM. Cu^{2+}, Cd^{2+}, and Ni^{2+} all inhibited mOTOP3 currents to varying degrees, with Cu^{2+} serving as the most potent inhibitor (**Figure 5—figure supplement 1**). Importantly, Ni^{2+}
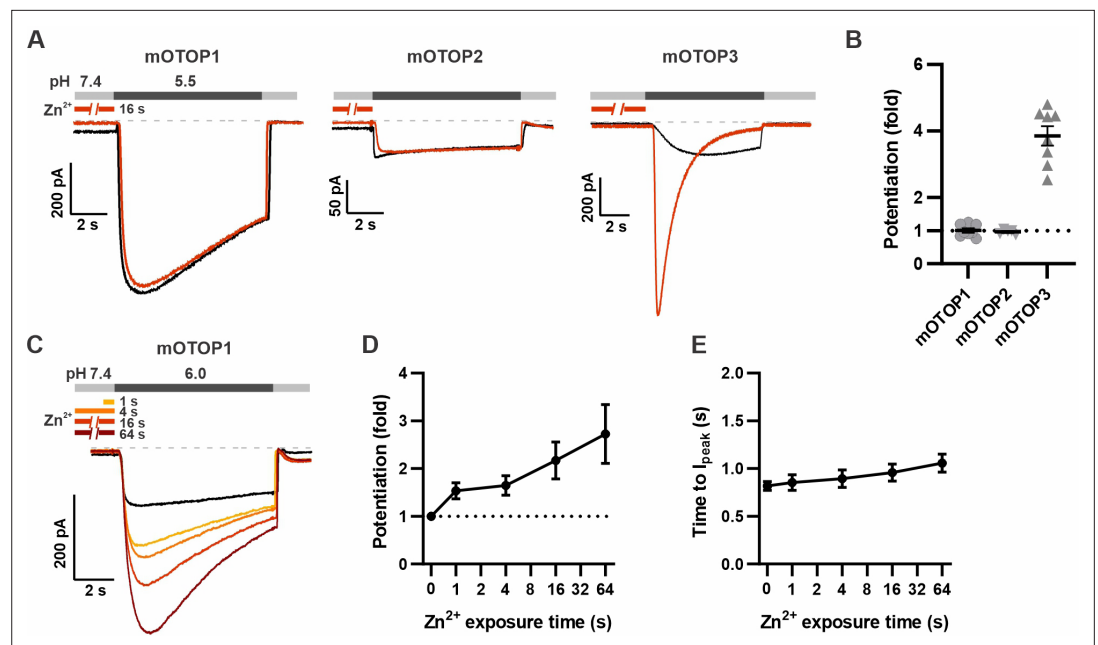
Figure 4. mOTOP1 is potentiated by Zn^{2+} when activated by a mild acid stimulus. (**A**) Proton currents recorded from HEK293 cells expressing each of the three mOTOP channels as indicated, in response to pH 5.5 with (red) or without (black) Zn^{2+} pre-exposure. V_m was held at –80 mV. The cells were exposed to 1 mM Zn^{2+} for 16 s prior to pH 5.5 solutions. (**B**) Average and all points data from experiments as in (A) showing the fold potentiation in response to 1 mM Zn^{2+} for 16 s. (**C**) Representative traces showing mOTOP1 currents evoked in response to a pH 6.0 stimulus before and after exposure to Zn^{2+} for varying times as indicated. (**D, E**) The fold potentiation (**C**) and time to I_{peak} (**D**) as a function of Zn^{2+} pre-exposure time from experiments as in (C) (n=5). Data are plotted as mean ± s.e.m.

The online version of this article includes the following source data for figure 4:

Source data 1. Source data for *Figure 4*.

inhibited mOTOP3 currents to similar degree as Zn^{2+} but was a less potent activator. We conclude that the inhibitory and activating metal binding sites have different ligand specificity, consistent with the interpretation that they are distinct (see below).

The tm 11-12 linker is necessary and sufficient to confer sensitivity to Zn^{2+} potentiation

Given the marked difference between mOTOP3 and mOTOP2 in potentiating effects of Zn^{2+}, we reasoned that chimeras between the two channels might allow us to identify its structural basis. As Zn^{2+} is likely to bind to an extracellular domain, we tested chimeras in which each of the six external linkers between transmembrane domains were exchanged (*Teng et al., 2022*). A total of twelve chimeras were tested, six in which the backbone was the mOTOP2 channel and six in which the back-bone was the mOTOP3 channel. Each chimera was tested for potentiation following pre-exposure to 1 mM Zn^{2+} for 16 s (*Figure 6*).

Strikingly, we found that Zn^{2+} potentiation was eliminated in a chimera containing the mOTOP3 backbone with the tm 11–12 linker from mOTOP2 (O3/O2(L11-12); *Figure 6B, C and E*). Indeed, even a 64 s exposure to 1 mM Zn^{2+} had no effect on the magnitude or activation kinetics of the currents (*Figure 6—figure supplement 1*). Interestingly, the O3/O2(L11-12) chimera is activated at a higher pH and currents are more rapidly activating than currents carried by mOTOP3 (*Figure 6B* and *Teng et al., 2022*). This suggests that the O3/O2(L11-12) channels may be partly locked in a potentiated state. None of the other chimeras with a mOTOP3 backbone showed a loss of potentiation.

Remarkably, simply transplanting the 11–12 linker from mOTOP3 onto mOTOP2 (O2/O3(L11–12)) conferred sensitivity to potentiation by Zn^{2+}. Notably, pre-exposure of O2/O3(L11–12) channels to 1 mM Zn^{2+} for 16 s caused a nearly fourfold potentiation of the subsequent currents evoked in response to a pH 5.5. stimulus (*Figure 6A, C and D*). The other five chimeras containing an mOTOP2 backbone remained
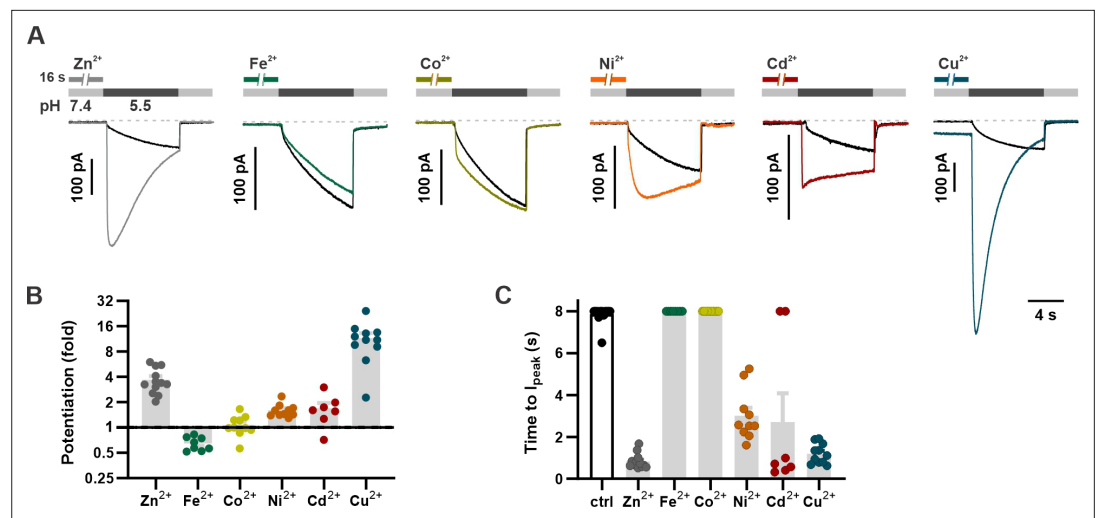
Figure 5. Divalent transition metal ions also potentiate mOTOP3. (**A**) Proton currents in response to a pH 5.5 stimulus following exposure (1 mM, 16 s) to various d-block transition metals recorded from HEK293 cells expressing wildtype mOTOP3. V_m was held at –80 mV. Black trace is the control from the same experiment (cell). (**B**) Average (mean ± s.e.m.) and all points data showing the fold potentiation measured from experiments as in (**A**). (**C**) Average (mean ± s.e.m.) and all points data for latency to I_{peak}, measured from experiments as in (A). The latency to peak in (C) was scored as 8 s when peak magnitudes were not reached before 8 s.

The online version of this article includes the following source data and figure supplement(s) for figure 5:

Source data 1. Source data for *Figure 5*.

Figure supplement 1. Divalent transition metals also inhibit mOTOP3.

Figure supplement 1—source data 1. Source data for *Figure 5—figure supplement 1*.

resistant to Zn^{2+} potentiation. Zn^{2+} potentiation of O2/O3(L11–12) showed a time dependence similar to that of wildtype mOTOP3 channels (*Figure 6F and G*). mOTOP2 and O2/O3(L11–12), but not mOTOP3, carry outward currents in response to alkaline stimuli (*Teng et al., 2022*). Thus, we wondered if the sensitivity to potentiation by Zn^{2+} would be observed for outward currents. Following exposure to 1 mM Zn^{2+} for 16 s, currents elicited in response to a pH 9.0 stimulus were smaller than in the absence of Zn^{2+} for both WT and O2/O3(L11–12) channels (*Figure 6H*). We conclude that the 11–12 linker contributes to the potentiation of OTOP channels by Zn^{2+} in response to acidic but not alkaline stimuli.

While none of the other chimeras containing an mOTOP3 backbone showed a reduction in Zn^{2+} potentiation, several showed an increase (*Figure 6C and E*). Interestingly, a chimera with a swap of the tm 1–2 linker, O3/O2(L1–2), which was previously observed to be non-conductive in response to changes in extracellular pH (*Teng et al., 2022*), was strongly activated by Zn^{2+}. Thus, for this chimeric channel, the increase in fold potentiation mostly reflects the large decrease in the acid-induced currents, rather than an increase in the magnitude of the currents after Zn^{2+} exposure and suggests that the 1–2 linker plays a role in acid activation of mOTOP3.

To determine if potentiating and inhibiting effects of Zn^{2+} were mediated by the same binding site, we next tested whether currents carried by O3/O2(L11–12) and other mOTOP3 chimeras retained sensitivity to inhibition by Zn^{2+} following activation at pH 5.5 (*Figure 7*). All chimeras were inhibited by 1 mM Zn^{2+}, including the O3/O2(L11–12) chimera, although the extent of the inhibition, which ranged from ~40% to 80%, varied significantly between some of the chimeras and WT channels (*Figure 7*). Interestingly, potentiation following Zn^{2+} inhibition was absent not just in the O3/O2(L11–12) chimera, as expected, but also in the O3/O2(L3–4) chimera which showed potentiation with the pre-exposure protocol. This suggests that while differences in L3–4 do not account for differences in Zn^{2+} potentiation between mOTOP2 and mOTOP3, residues in L3–4 may nonetheless contribute to activation of the channels.

Together we conclude that the mOTOP3 11–12 linker is both necessary and sufficient to confer sensitivity to potentiation by Zn^{2+}. Other parts of the channel may contribute to gating by Zn^{2+} either directly or through allosteric effects.
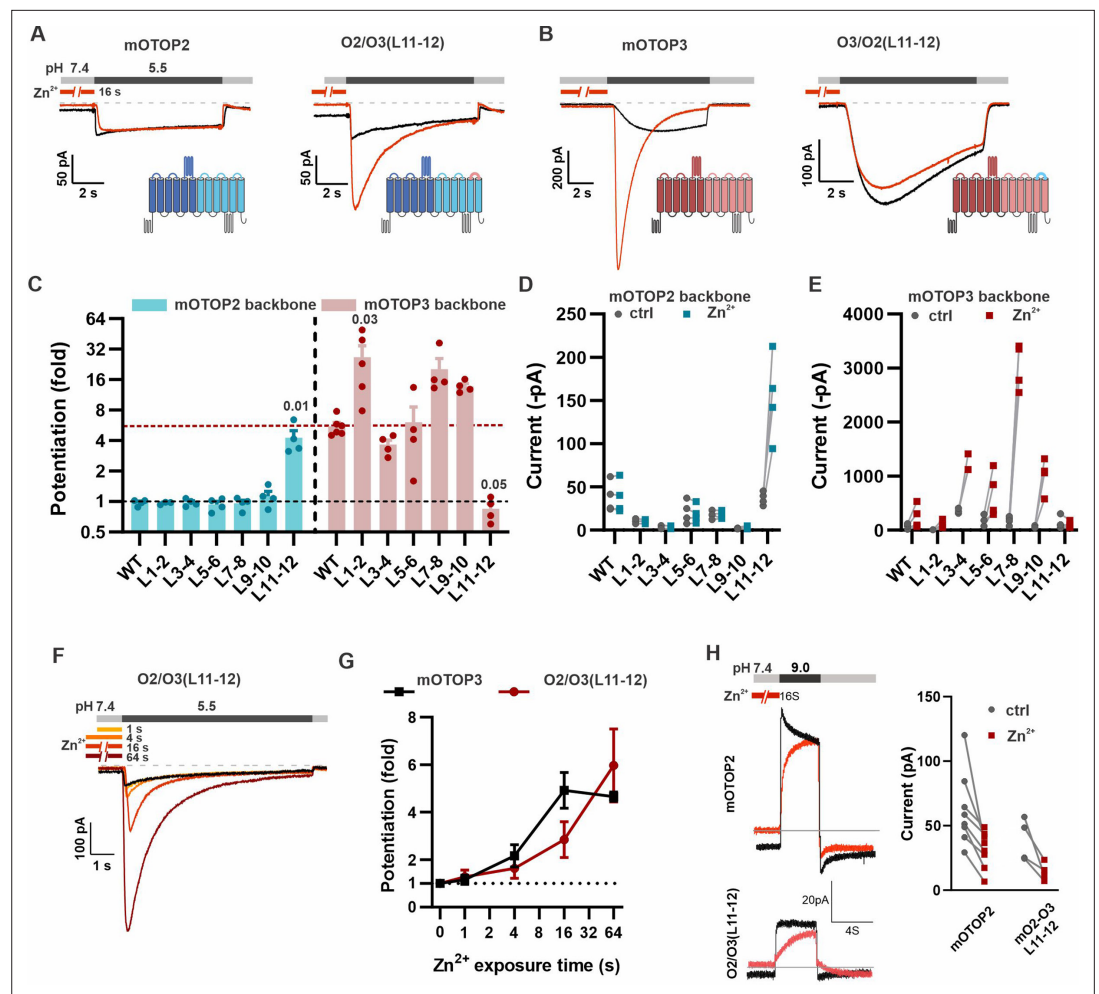
Figure 6. The tm 11–12 linker is both necessary and sufficient for Zn^{2+} potentiation. (**A, B**) Proton currents in response to a pH 5.5 stimulus with (red) or without (black) Zn^{2+} pre-exposure (1 mM, 16 s) recorded from HEK293 cells expressing either wildtype (WT) OTOP channels or chimeric channels as indicated. V_m was held at –80 mV. The WT traces are the same set as shown in *Figure 3A*. (**C**) Average data showing the fold potentiation after Zn^{2+} pre-exposure (1 mM, 16 s) measured from experiments as in (**A**) and (**B**). Bars are mean ± s.e.m. mOTOP2 and its chimeras are shown in blue, mOTOP3 and its chimeras are shown in red. Statistical significance determined with an ANOVA using Kruskal-Wallis (non-parametric) statistics. P values are shown where less than 0.05. (**D, E**) Same data as in (**C**) plotted to show current magnitudes before and after Zn^{2+} for WT channels and each of the chimeras. (**F**) Representative traces of O2/O3(L11-12) currents in response to pH 5.5 after pre-exposure to Zn^{2+} for varying times as indicated. (**G**) Average data for experiments as in (**F**) showing the time dependence of the potentiation by Zn^{2+} for the O2/O3(L11-12) chimera as compared with WT (n=4–5). Data of the WT mOTOP3 are the same set as shown in *Figure 2C and D*. (**H**) Left panel: response of mOTOP2 to alkaline stimulus (pH 9.0) with (red) and without (black) Zn^{2+} pre-exposure (1 mM, 16 s). Right panel: magnitude of currents at pH 9 for WT and mutant channels with and without Zn^{2+} pre-exposure. Currents were smaller after Zn^{2+} pre-exposure for both.

The online version of this article includes the following source data and figure supplement(s) for figure 6:

Source data 1. Source data for *Figure 6*.

Figure supplement 1. O3/O2(L11-12) chimera is completely insensitive to potentiation by Zn^{2+}.

Figure supplement 1—source data 1. Source data for *Figure 6—figure supplement 1*.

Contribution of H531 and other residues to Zn^{2+} potentiation

The tm 11–12 linker is relatively short, consisting of sixteen amino acids, of which five are conserved between the three murine OTOP channels (*Figure 8A*). In this region, the residues that could coordinate Zn^{2+} and that vary between mOTOP3 and mOTOP2 are H531, E533, and E535 (mOTOP3

numbering, *Figure 8A*). Within mOTOP3, we mutated each residue to that found in mOTOP2 or to alanine. Strikingly, mutation of H531 to either arginine (found in mOTOP2) or alanine eliminated the ability of Zn^{2+} to potentiate mOTOP3 currents, assessed by measuring either the magnitude of the currents or their activation kinetics (*Figure 8B-D*). However, the converse was not true: introducing histidine at the same position in mOTOP2 (R517H) was not sufficient to produce potentiation by Zn^{2+} under the conditions tested (*Figure 8—figure supplement 1*). mOTOP1 has an arginine at the equivalent residue to H531, but is still potentiated by Zn^{2+}, albeit more weakly. Mutation to histidine at this position in OTOP1 (R554H) was sufficient to significantly increase Zn^{2+} potentiation (*Figure 8—figure supplement 1*).

Taken together, we conclude that H531 is a critical element of the Zn^{2+} activating site in mOTOP3. However, the complete binding site is undoubtedly formed by multiple residues that together coordinate Zn^{2+}. We, therefore, set out to identify these residues. Mutation of the acidic residues (E533 and E535) within the L11–12 linker had more subtle effects: mutation to residues found in mOTOP2 (H and S, respectively) had no effect on potentiation while mutation of E535 to alanine significantly reduced, but did not eliminate, potentiation (*Figure 8E-H*). Thus, the potentiation of mOTOP3 by Zn^{2+} may involve contributions, either direct or indirect, from both H531 and E535 in the tm 11–12 linker, and the relative contribution of each residue may vary between different channels and under different conditions.

Inspection of the structure of mOTOP3 predicted by AlphaFold (*Jumper et al., 2021*) reveals a possible Zn^{2+} binding site formed by H531, E535, and residues in the linker between tm 5–6, H234, and E238 (*Figure 9B*). Note that a histidine at the position equivalent to 234 (mOTOP3 numbering) is conserved among all murine OTOP channels while glutamic acid is present at a position equivalent to 238 in mOTOP1 (*Figure 9A*). To test the contributions of these residues to Zn^{2+} potentiation, we mutated each alone or in combination to alanine. The single mutations H234A and E238A each showed significantly reduced potentiation (3.5±0.64 and 2.4±0.12-fold potentiation, respectively) as compared with wildtype (10.0±1.0-fold) and the double mutation, H234A/E238A showed a further reduction in potentiation (1.3±0.21) as compared with either of the single mutants (*Figure 9F and G*). Interestingly, all mutants retained some degree of potentiation, and current activation was faster after Zn^{2+} exposure, which was not observed for the mOTOP3 H531A/R single mutation or the mO3_mO2_L11-12 chimera (*Figure 8D* and *Figure 6—figure supplement 1C*).

The data collectively demonstrate that gating of OTOP channels is regulated by Zn^{2+} acting through residues within the tm 11–12 and tm 5–6 linkers.

Kinetic model for Zn^{2+} potentiation

These data suggest that Zn^{2+} may act to lock the channel in an open state, possibly by binding more strongly to the same site that is titrated by H^+ ions to activate the channel (*Teng et al., 2022*). The data also suggest that a separate site with a faster off-rate mediates inhibition by Zn^{2+}. Thus, in the presence of Zn^{2+}, the channels may enter a state that is simultaneously activated (open gate) and inhibited. Upon removal of Zn^{2+}, the channels may then transit through a fully open state, as the inhibition is relieved faster than the activation. To formally test these predictions, we generated a kinetic model reflecting these properties and asked if it could recapitulate our experimental observations.

We postulated a model comprised of interacting elements that can each transition between two configurations: a pore gate that is either closed or open, a binding site for protons, and two types of binding sites for Zn^{2+} (one activating and one blocking), that are either unoccupied or occupied (*Figure 10A*). For a detailed description of this type of model representation, see *Goldschen-Ohm et al., 2014*. The proton and activating Zn^{2+} sites are energetically coupled to the pore such that binding speeds pore opening and/or slows pore closing. To model the competition of protons and Zn^{2+} for the same activating site(s), we destabilized all states where both the proton and activating Zn^{2+} sites are simultaneously occupied. We modeled the blocking Zn^{2+} site as independent of all other model elements, except that when occupied all channel current is blocked. Simulated currents in response to the same pH and Zn^{2+} protocols used in our experiments qualitatively describe our observed mOTOP3 current responses (*Figure 10B and C*), supporting the plausibility of our proposed mechanism. For example, the model recapitulates the rebound following addition and removal of Zn^{2+} during an acid stimulus. It also recapitulates the speeding up of current activation for a pre-exposure to Zn^{2+} at 0.3 mM, and the increase in current magnitudes with pre-exposure to Zn^{2+} at 1 and 3 mM.
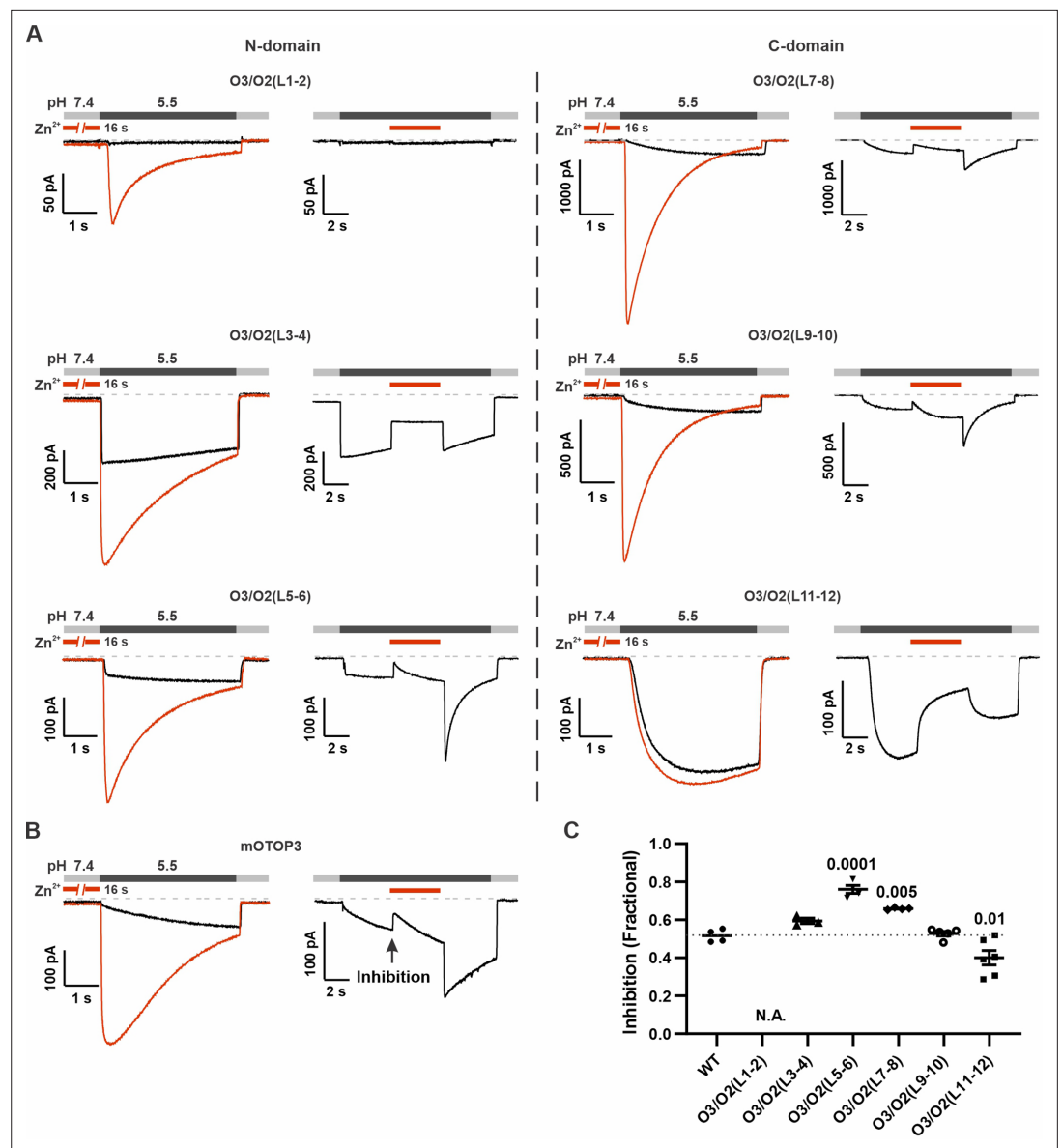
Figure 7. Inhibition of mOTOP3 by Zn^{2+} is retained in chimeric channels. (**A**) Zn^{2+} sensitivity of chimeric mOTOP3-mOTOP2 channels as measured with a pre-exposure protocol (left panel in each) or by adding 1 mM Zn^{2+} to the pH 5.5 stimulus (blocking protocol; right panel in each). Chimeras containing mOTOP2 N-domain and C-domain linkers are shown in the left column and right columns, respectively. Data from pre-exposure experiments is also presented in *Figure 6*, and here is shown for comparison to results with the blocking protocol. (B) Representative traces of wildtype mOTOP3 currents in response to the same protocols as in (**A**). The arrow indicates the time point in this trace where inhibition by Zn^{2+} was measured, by comparison with the current magnitude before adding Zn^{2+}. (**C**) Average (mean ± s.e.m.) and all points data showing fractional inhibition of currents by 1 mM Zn^{2+} measured from wildtype mOTOP3 and its chimeras. All channels were similarly inhibited by 1 mM Zn^{2+}. Significance determined by ANOVA with Dunnett's test corrected for multiple comparisons.

The online version of this article includes the following source data for figure 7:

Source data 1. Source data for *Figure 7*.

It also qualitatively recapitulates the decay of the potentiated currents, which in the model is due to unbinding of the Zn^{2+} (see *Figure 10—figure supplements 1–3*). Conceptually, upon occupancy of the activating site by Zn^{2+} the channel will enter a potentiated state, and thereafter upon removal of Zn^{2+} the channel will slowly return to its baseline activity in the absence of Zn^{2+} with a time course that is largely described by the time course of Zn^{2+} unbinding from the activating site (*Figure 10—figure*

supplement 2). We note that such a decay could potentially also reflect a desensitization or ion accumulation process which we did not attempt to model.

However, this model also undoubtedly represents an oversimplification of the true number and properties of the states the channel adopts. For example, the model does not recapitulate the observed decay of the currents below baseline when strongly potentiated, which may reflect contributions from an inactivation process or ion accumulation not modeled. Making things more complicated, and interesting, it is also entirely possible that there is more than one permeation pathway and gate (*Chen et al., 2019*; *Saotome et al., 2019*), and that Zn^{2+} opens one of the permeation pathways and not the other. The 11–12 loop sits close to the intrasubunit interface, so that at present it is not possible to predict if it would open a permeation pathway in the N domain, the C domain, or the intrasubunit interface.

Discussion

The OTOP proton channels were discovered in 2018 when mOTOP1 was cloned from taste tissue as a putative sour receptor (*Tu et al., 2018*). At that time, mOTOP1 was shown to have near-perfect selectivity for protons over other ions, and to generate inward currents as the pH was lowered. Vertebrate OTOP2 and OTOP3, as well as invertebrate channels also carry inward proton currents in response to extracellular acidification, and where tested have been shown to function as proton-selective ion channels (*Tu et al., 2018*; *Chen et al., 2019*) (see also *Teng et al., 2022*). Nearly all descriptions regarding the functional properties of OTOP channels come from the heterologous expression of OTOP channels and save for the description of proton currents now attributed to mOTOP1 channels in taste cells (*Chang et al., 2010*; *Bushman et al., 2015*), all descriptions of OTOP channels postdate the discovery of the genes encoding the proton channels. That is, even by scouring the literature, it is difficult to find a description of a proton current that could be attributed to an OTOP channel in a native cell type. Thus, in contrast to K^+ channels where there was a vast literature regarding their functional properties before their cloning, for OTOP channels, this kind of information was not available.

Critically, before this work and that described in *Teng et al., 2022*, it was not known if OTOP channels were gated, and if so by what. Here, we provide evidence that OTOP channels are gated by Zn^{2+} and other transition metals. In the apo, Zn^{2+}-free condition, mOTOP3 currents are small and slowly activating. With pre-exposure to 1–3 mM Zn^{2+} for several seconds, the currents increase in magnitude by up to 10-fold. This can only be explained if Zn^{2+} either increases the probability that the channels open or produces a change in their conductance – gating them. We also find that pre-exposure to copper (Cu^{2+}) strongly potentiates OTOP3 currents. Together with other recent evidence for pH-dependent gating (*Teng et al., 2022*), we can now say with certainty that some OTOP channels are gated.

Structural considerations

The structures of two of the three OTOP channels have been reported at near-atomic resolution ([zebrafish OTOP1, chicken OTOP3, and *Xenopus* OTOP3; *Chen et al., 2019*; *Saotome et al., 2019*)]. In addition, predictions are available for structures of mouse and human OTOP channels that appear to be reliable (*Jumper et al., 2021*; *Teng et al., 2022*; *Varadi et al., 2022*). All the structures to date share common features: The protomers assemble as dimers, and each protomer shows a twofold symmetry, leading to an overall pseudo-tetrameric stoichiometry. The four pseudo-subunits come together to form a central cavity that is filled with lipids and cannot support ion permeation. Instead, ions may permeate through the barrel-like structures formed from transmembrane domains 2–6 (N domain) and 8–12 (C domain) or at the intrasubunit interface (formed mostly by tm 6 and 12). From these static structures, it is not possible to tell if the channels are gated, and if so, what state they are
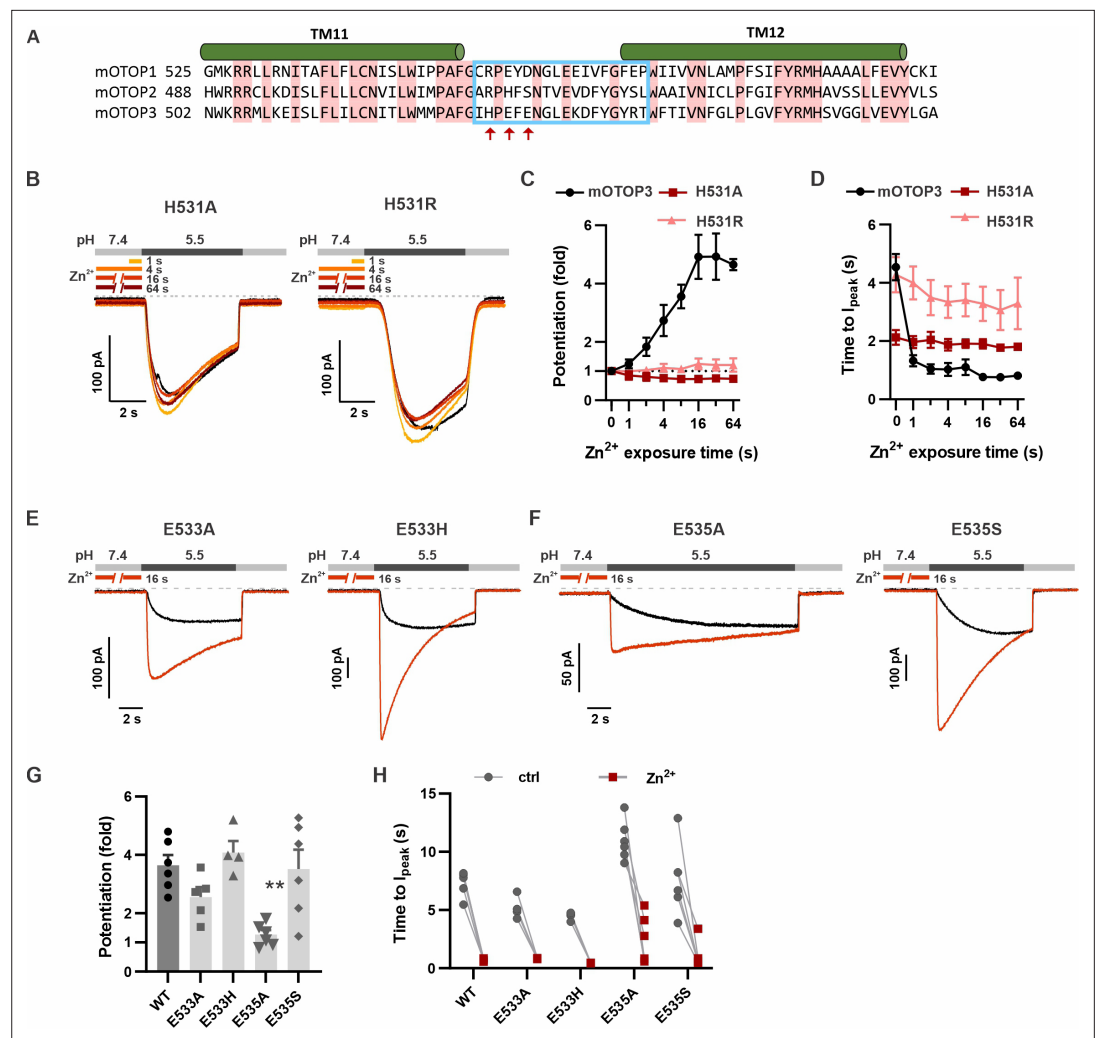
Figure 8. H531 in mOTOP3 L11–12 is essential for Zn^{2+} potentiation. (**A**) Sequence alignment of three mOTOP channels. The residues that were exchanged between mOTOP2 and mOTOP3 in the L11–12 chimeras is indicated with a blue box. Residues that differed between the two channels and that were tested are indicated by red arrows. (**B**) Representative traces of mOTOP3_H531A and H531R currents in response to pH 5.5 after pre-exposure to Zn^{2+} for varying times as indicated. (**C, D**) Average data for fold potentiation (**C**) and latency to I_{peak} (**D**) measured from experiments as in (B), plotted as a function of pre-exposure time to Zn^{2+} (n=3–7). Data from wildtype (WT) mOTOP3 are the same set as shown in *Figure 2C and D*. (**E, F**) Responses of mOTOP3 mutants as indicated in response to pH 5.5 with (red) or without (black) Zn^{2+} pre-exposure (1 mM, 16 s). V_m was held at –80 mV. (**G**) Average data for fold potentiation measured from experiments as in (E and F). Statistical significance compared with WT determined using the Kruskal-Wallis (non-parametric) test corrected for multiple comparison. (**H**) Latency to peak currents of WT mOTOP3 or mutant currents, measured from experiments as in (**E and F**). Each set of points represents a separate cell.

The online version of this article includes the following source data and figure supplement(s) for figure 8:

Source data 1. Source data for *Figure 8*.

Figure supplement 1. Introduction of histidine into mOTOP1 partially confers sensitivity to potentiation by Zn^{2+}.

Figure supplement 1—source data 1. Source data for *Figure 8—figure supplement 1*.

in (open or closed). Based on the pH sensitivity of the channels (*Teng et al., 2022*), we presume they are closed.

We have focused on mOTOP2 and mOTOP3, which show the most divergent functional properties. In addition to differences in the effects of Zn^{2+} described here, we have also described differences in pH sensitivity of the two channels (*Teng et al., 2022*). mOTOP3 is gated by protons, and thus

conducts currents only in response to extracellular acidification (<pH 5.5), while OTOP2 is constitutively open and conducts currents over a large pH range, including outward currents when the extracellular solution is alkalinized. The strikingly different functional properties of the two channels, but otherwise overall similar architecture, provided us the opportunity to identify motifs involved in gating using a chimeric approach.

Remarkably, we found that a short stretch of amino acids linking transmembrane domains 11–12 was necessary for Zn^{2+} potentiation of mOTOP3 and sufficient to confer Zn^{2+}-sensitive gating on mOTOP2. Within that stretch, we identified one amino acid, H531, mutations of which (to R or A)
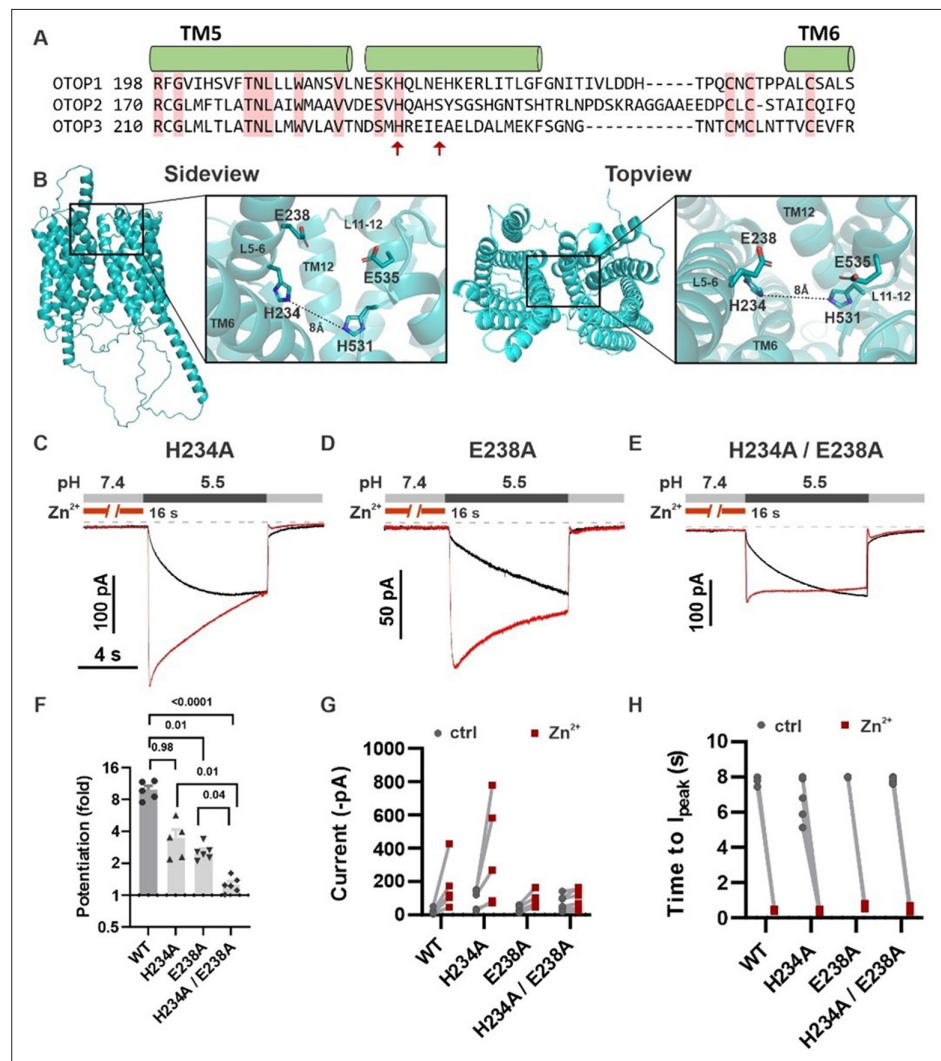

Figure 9. H234 and E238 in transmembrane domain 5 contribute to Zn^{2+} potentiation of mOTOP3. (**A**) Sequence alignment of the three mOTOP channels. Alpha helices shown above the sequence are based on the AlphaFold prediction of the structure of mOTOP3. Red arrows indicate residues neutralized to alanine in subsequent experiments. (**B**) Images generated using the AlphaFold predicted structure of mOTOP3. Left panel shows a sideview and right panel shows a topview of mOTOP3. Each zoom-in highlights the predicted Zn^{2+} potentiation binding site. (**C,D,E**) Representative traces of mOTOP3 H234A, E238A, and a double mutation of H234A/E238A in response to lowering the extracellular pH to 5.5 after (red) and without (black) pre-exposure to Zn^{2+} (1 mM, 16 s). V_m was held at –80 mV. (**F**) Average (mean ± s.e.m.) and all points data showing the fold potentiation measured from experiments as in (**C,D,E**). Statistical significance determined using an ANOVA with the Kruskal-Wallis (nonparametric) test. (**G,H**) Same data as in (**F**) plotted to show current magnitudes before and after Zn^{2+} (**G**) and the time to I_{peak} with and without pre-exposure to Zn^{2+} (**H**) from experiments in (**C,D,E**).

The online version of this article includes the following source data for figure 9:
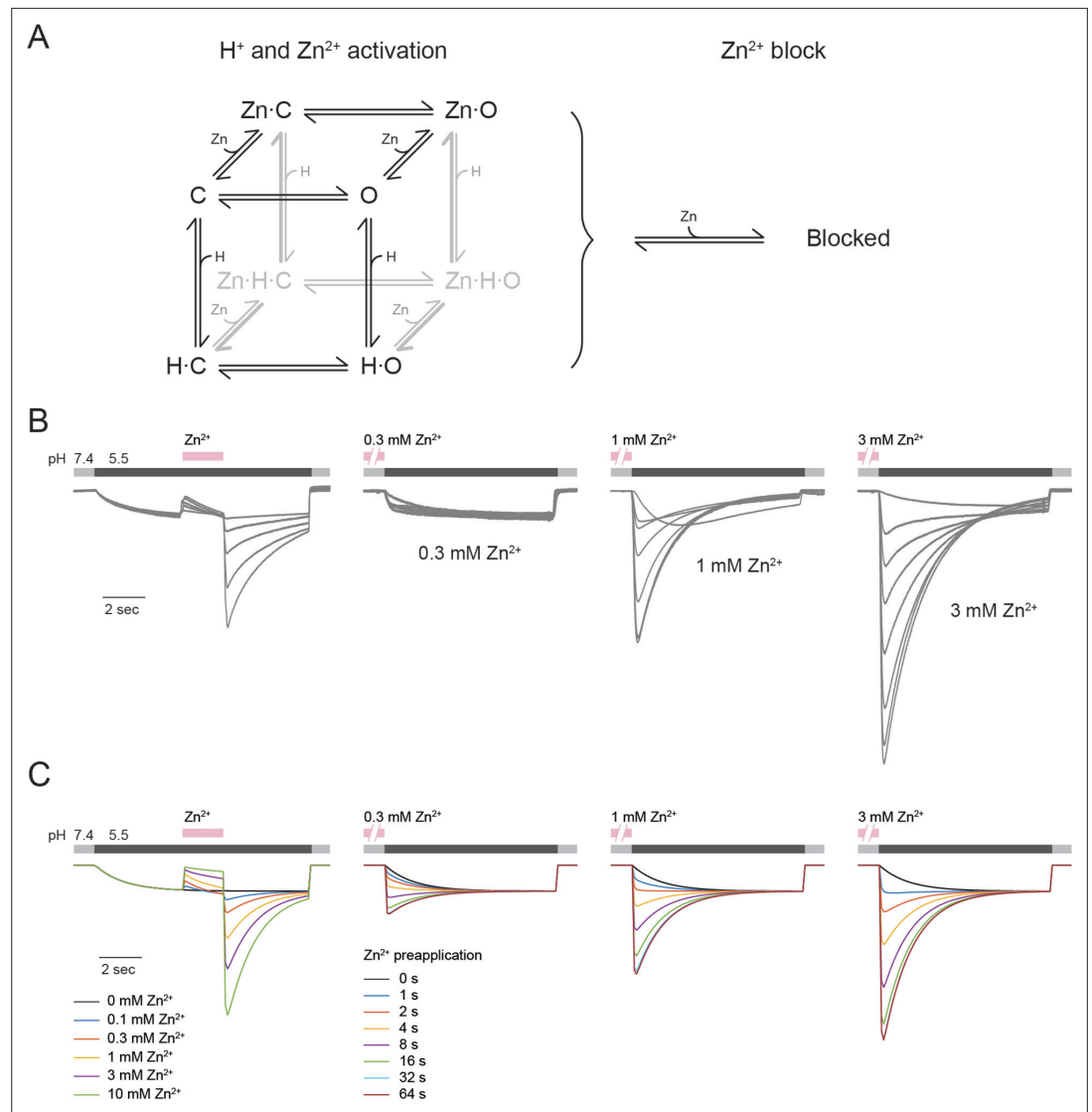
Source data 1. Source data for *Figure 9*.

Figure 10. mOTOP3 kinetic model for Zn^{2+} potentiation and block. (**A**) Kinetic model for activation of mOTOP3 by H$^+$ and Zn^{2+}. The channel moves from a closed state (**C**) upon binding H$^+$ or Zn^{2+} to an open state (Zn-O, H–O) in which it permeates protons. The doubly bound Zn-H-O and Zn-H-C states are disfavored energetically. A separate site binds Zn^{2+} and inhibits channel permeation, independently of the gating state. See methods for a more detailed description of the model. (**B**) Example mOTOP3 current recordings from *Figure 1C* and *Figure 2B*. Each set of recordings was from a different cell. (**C**) Simulated currents for the model under the same protocols as in (B). Model parameters were adjusted manually and were the same for all traces. The model replicates the rebound seen upon addition of Zn^{2+} at pH 5.5, and the potentiation seen with pre-exposure to Zn^{2+} at pH 7.4.

The online version of this article includes the following figure supplement(s) for figure 10:

Figure supplement 1. Simulation time course for individual gating and binding domains in response to a pulse of Zn^{2+} during an acid stimulus.

Figure supplement 2. Simulated decay of current potentiation largely reflects Zn^{2+} unbinding from the activating site.

Figure supplement 3. Simulation time course for individual gating and binding domains in response to an acid stimulus following pre-exposure to Zn^{2+}.

completely abolished Zn^{2+}-sensitive gating in mOTOP3. As histidine is well documented to form part of the Zn^{2+} binding site in other Zn^{2+}-sensitive proteins (*Vallee and Auld, 1990*), including the voltage-gated proton channel HV1 (*Ramsey et al., 2006*), H531 likely contributes to coordinating Zn^{2+} in mOTOP3. However, Zn^{2+} is typically coordinated by sidechains of four or more residues, which in addition to the imidazole rings of histidine, includes sulfhydryl groups of cysteine, carboxyl group of acidic residues (aspartic and glutamic acid). Moreover, water can also participate in coordinating Zn^{2+} (*Vallee and Auld, 1990*). In addition to H531, we have identified three other residues, H234, E238, and E535, that when mutated to alanine lead to reduced efficacy of Zn^{2+} to potentiate mOTOP3. Based on the functional data provided in this paper and an AlphaFold structure of mOTOP3, we tentatively predict these four residues form the Zn^{2+} activating binding site. Interestingly, alkali activation of mOTOP1 was recently shown to require a basic residue at a position equivalent to H531 in mOTOP3 and in the tm 11–12 linker at a position close to H234 (*Tian et al., 2023*). It is tempting to speculate that Zn^{2+} binding could bring together residues in the tm 5–6 linker and tm 11–12 linker that are at a distance in the closed state (8 Å; *Figure 9B*) to stabilize an open state, as shown for other ion channels (*Gordon and Zagotta, 1995b*; *Zhang et al., 2009*). A similar mechanism could open mOTOP1 channels in response to alkaline pH.

Role of zinc in health and disease

Zinc is required for the functioning of a wide range of enzymes and proteins in the body and supplementary zinc has both beneficial and detrimental health effects. Given that it is mostly not known which cells express OTOP channels, or what functions they play in those cells, it is hard to predict the functional role of Zn^{2+}-sensitive gating in physiology. The dual blocking and potentiating effect of Zn^{2+} make it likely that the enhanced activity would be mostly evident under conditions where Zn^{2+} concentrations dropped rapidly or that favored binding of Zn^{2+} to its activating site over its blocking site. These studies also raise the interesting prospect that other molecules could be found that function as positive allosteric modulators of OTOP channels, with selectivity for the activating site over the blocking site, and that could ameliorate effects of reductions in OTOP channel function that lead to vestibular or other disorders.

Materials and methods

Key resources table

Reagent type (species) or resource	Designation	Source or reference	Identifiers	Additional information
Gene (*Mus musculus*)	*Otop1, Otop2,* and *Otop3*	*Tu et al., 2018*. PMID:29371428		
Cell line (*Homo sapiens*)	HEK293	ATCC	CRL-1573	
Cell line (*Homo sapiens*)	PAC-KO HEK293 cells	*Yang et al., 2019*. PMID:31023925		
Recombinant DNA reagent	*Otop1, Otop2* and *Otop3* in pcDNA3.1	*Tu et al., 2018*. PMID:29371428		
Recombinant DNA reagent	*Otop1, Otop2* and *Otop3* – GFP	*Saotome et al., 2019*. PMID:31160780		
Recombinant DNA reagent	mO2_O3 loop swap mutations	This paper		cDNAs encode chimeric channels (see Materials and methods and *Figure 6—figure supplement 1*). Available upon request
Recombinant DNA reagent	mO3_O2 loop swap mutations	This paper		cDNAs encode chimeric channels (see Materials and methods and *Figure 6—figure supplement 1*). Available upon request
Recombinant DNA reagent	pHluorin in pcDNA3	Miesenbock, et al., 1998. PMID:9671304		
Chemical compound, drug	CHES	Sigma	C2885	
Chemical compound, drug	PIPES	Sigma	P6757	
Chemical compound, drug	Homopiperazine-1,4-bis(2-ethanesulfonic acid)	Sigma	53588	

Continued on next page

Continued

Reagent type (species) or resource	Designation	Source or reference	Identifiers	Additional information
Software, algorithm	GraphPad Prism 8 and 9	GraphPad	RRID:SCR_002798	
Software, algorithm	pClamp and clampfit	Molecular Devices	RRID:SCR_011323	
Software, algorithm	Origin	OriginLab corporation	RRID:SCR_002815	
Software, algorithm	CorelDraw	Corel	RRID:SCR_014235	
Software, algorithm	SimplePCI	HCImage	https://hcimage.com/simple-pci-legacy/	

Clones, cell lines, and transfection

Mouse OTOP1, OTOP2, and OTOP3 cDNAs were in a pcDNA3.1 vector with an N-terminal fusion tag consisting of an octahistidine tag followed by eGFP, a Gly-Thr-Gly-Thr linker, and 3C protease cleavage site (LEVLFQGP) were as previously described (*Saotome et al., 2019*). All chimeras and mutations were generated using In-Fusion Cloning (Takara Bio) and were confirmed by Sanger sequencing (Genewiz) (see *Teng et al., 2022*).

HEK293 cells were purchased from ATCC (CRL-1573). The cells were cultured in a humidified incubator at 37°C in 5% CO_2 and 95% O_2. The high glucose DMEM media (Thermo Fisher) is implemented with 10% fetal bovine serum (Life Technology) and 1% penicillin-streptomycin antibiotics. Cells were passaged every 3–4 days. Cells were tested and found free of mycoplasma using a PCR detection kit (Sigma-Aldrich, USA).

Cells used for patch-clamp recordings were transfected in 35 mm Petri dishes, with 600–1000 ng DNA and 2 μL TransIT-LT1 transfection reagents (Mirus Bio Corporation) following the manufacturer's protocol. After 24 hr, the cells were lifted using trypsin-EDTA and plated into a recording chamber.

Patch-clamp electrophysiology

Whole-cell patch-clamp recording was performed as previously described (*Teng et al., 2019*). Briefly, recordings were obtained with an Axonpatch 200B amplifier, digitized with a Digidata 1322a 16-bit data acquisition system, acquired with pClamp 8.2, and analyzed with Clampfit 9 or 10 (Molecular Devices). Records were sampled at 5 kHz and filtered at 1 kHz. Patch pipettes with a resistance of 2–4 MΩ were fabricated from borosilicate glass (Sutter Instrument). Solution exchange was achieved with a fast-step perfusion system (Warner Instrument, SF-77B) custom modified to hold seven microcapillary tubes in a linear array. Cells were treated with trypsin-EGTA and plated into the recording chamber immediately before each experiment. After a gigaohm seal was formed and whole-cell recording was achieved, the cell was lifted and moved in front of the microcapillary tubes. The membrane potentials were held at −80 mV unless otherwise indicated.

Patch-clamp electrophysiology solutions

Tyrode's solution contained 145 mM NaCl, 5 mM KCl, 1 mM $MgCl_2$, 2 mM $CaCl_2$, 20 mM dextrose, 10 mM HEPES (pH adjusted to 7.4 with NaOH). Standard pipette solution contained 120 mM Cs-aspartate, 15 mM CsCl, 2 mM Mg-ATP, 5 mM EGTA, 2.4 mM $CaCl_2$ (100 nM free Ca^{2+}), and 10 mM HEPES (pH adjusted to 7.3 with CsOH; 290 mOsm). Standard Na^+-free extracellular solutions contained 160 mM NMDG, 2 mM $CaCl_2$, and 10 mM buffer (HEPES for pH 7.4, MES for pH 6.0 and 5.5), and pH was adjusted with HCl to 7.4.

$ZnCl_2$ was directly introduced into the Na^+-free solutions where the final concentration was less than 3 mM, which caused a change in osmolarity of <10 mOsm. The pH was re-adjusted with NMDG-OH or HCl as needed. For the experiment in *Figure 1C*, the concentration of NMDG in the 10 mM Zn^{2+} solution was reduced to maintain an ~300 mOSM osmolarity.

For experiments in *Figure 5* and *Figure 5—figure supplement 1*, $FeCl_2$, $CoCl_2$, $NiCl_2$, $CuCl_2$, and $CdCl_2$ were directly introduced into the Na^+-free solutions at a concentration of 1 mM immediately before the experiment was performed. The pH was re-adjusted with NMDG-OH or HCl as needed.

Quantification and statistical analysis

All data are presented as mean ± SEM if not otherwise noted. Statistical analysis was performed using GraphPad Prism 9 (GraphPad Software Inc). The sample sizes of 3–10 independent recordings from individual cells per data point are similar to those in the literature for similar studies. For comparison of fold potentiation, an ANOVA was used with the Kruskal-Wallis (non-parametric) test (GraphPad Prism 9). All replicates are biological replicates. Number of replicates are indicated in the figure or figure legend. They represent recordings from different cells transfected with the same plasmid DNA. Data were excluded if a gigaohm seal was not established or maintained, as indicated by an inward current of >80 pA (–80 mV) in the presence of the OTOP channel blocker Zn^{2+} applied at pH 7.4. Data sets that represent time series were excluded if four or fewer time points were collected out of a possible eight time points, due to seal instability.

Representative electrophysiology traces shown in the figures were acquired with pClamp, and in some cases, the data was decimated by 10-fold before exporting into graphic programs, Origin (Microcal) and Coreldraw (Corel).

Kinetic modeling

A kinetic model was generated based on interacting binary elements as described in *Goldschen-Ohm et al., 2014*. Briefly, each element can adopt one of two possible configurations (closed or open for the pore, unbound or bound for each binding site) with intrinsic rate constants for transitioning between them. The elements are energetically coupled such that binding at a particular site either promotes or inhibits pore opening. To simulate competition between H^+ and Zn^{2+} for the activating site(s), occupation of one site energetically destabilizes the other.

Model parameters were manually adjusted to qualitatively recapitulate the experimental observations. Rate constants for pore opening/closing (k_o/k_c), proton binding/unbinding (k_{onH}/k_{offH}), Zn^{2+} binding/unbinding to activating sites (k_{onZnA}/k_{offZnA}) and blocking site (k_{onZnB}/k_{offZnB}) are (s^{-1} or $M^{-1}s^{-1}$ for binding rates): $k_o = 0.02$, $k_c = 25$, $k_{onH} = 5 \times 10^4$, $k_{offH} = 1$, $k_{onZnA} = 35$, $k_{offZnA} = 1$, $k_{onZnB} = 5 \times 10^4$, and $k_{offZnB} = 20$. In *Figure 10* these rates reflect the transition pairs from the unbound closed state C to either the unbound open state O (k_o, k_c) or each closed state having only a single binding site occupied (H·C, Zn·C, Blocked·C) (k_{onH}, k_{offH}, k_{onZnA}, k_{offZnA}, k_{onZnB}, k_{offZnB}). To describe how binding to a site influences pore opening and/or binding to other sites, and vice versa, we define state-dependent interaction energies between the pore gate and binding site domains. These energies modulate the rate constants as defined in *Goldschen-Ohm et al., 2014*. The interaction between the proton site and pore gate is such that proton binding reduces the energy barrier for pore opening by –4 kcal/mol without affecting pore closure. For example, this means that the transition rate from H·C to H·O will be exp(–(–4 kcal/mol)/RT)~850 times faster than that from C to O, where RT is the product of the molar gas constant R and temperature T and has value 0.593 kcal/mol at a room temperature of 298 K. Reciprocally, pore opening reduces the energy barrier for proton binding by –1 kcal/mol. These energetic effects imply that pore opening must also increase the barrier for proton unbinding by 3 kcal/mol (assuming transition rates are described by a single transition state energy barrier). The interaction between the activating Zn^{2+} site and pore gate is such that Zn^{2+} binding both reduces the energy barrier for pore opening by –3 kcal/mol and increases the barrier to pore closure by 3 kcal/mol, thereby increasing opening frequency and stabilizing the open pore. Reciprocally, pore opening reduces the barrier for Zn^{2+} binding to the activating site by –5 kcal/mol. These energetic effects imply that pore opening must also increase the barrier for Zn^{2+} unbinding from the activating site by 1 kcal/mol, thereby stabilizing bound Zn^{2+} at the activating site. To simulate competition between protons and Zn^{2+} for the activating site, states with both proton and activating Zn^{2+} sites occupied were destabilized by 6 kcal/mol, the value for which was simply chosen to be a

somewhat large destabilizing energy. The Zn^{2+} blocking site was assumed to be independent of all other elements, but when occupied blocks all channel current. This model includes 14 free parameters: eight rate constants describing the opening/closing of the pore gate and binding unbinding at the proton and Zn^{2+} activating and blocking sites, and six state-dependent interaction energies defining how activation/ occupation of the above elements influences the rates of the other elements. However, the model is relatively insensitive to some of the parameters (within reason). For example, binding/unbinding of Zn^{2+} from the blocking site is very fast in comparison to the macroscopic current kinetics of proton activation and decay of Zn^{2+} potentiation. Thus, any set of blocking kinetics that give a relatively rapid onset and offset of the block will likely perform similarly in the model.

For comparison with model simulations, the entire set of currents across all cells was uniformly scaled under the assumption that the maximal response following preapplication of 3 mM Zn^{2+} is reflective of channels with an open probability of ~0.9, a measure that has not been experimentally verified. It is likely that the same model structure will similarly describe responses with lower maximal open probabilities, albeit with slightly different parameter values. Given these uncertainties, as well as the relatively large number of free parameters (11 parameters defining pore gating, binding to activating sites, and their interactions are most relevant), we did not attempt to optimize the model parameters, but instead manually identified parameters that qualitatively recapitulate the data. The time-dependent probability in each state was simulated as described by *Colquhoun and Hawkes, 1995*, after first generating the matrix of transition rates between states from the model's binary elements and interactions (*Goldschen-Ohm et al., 2014*). Currents were computed from the simulated open probability assuming a conductance of 1 pS and a driving force of –80 mV in pH 5.5 and 0 in pH 7.4 as estimated from ramp experiments (*Teng et al., 2022*). The choice of conductance is arbitrary given that we do not know how many channels are in each recording, and thus only contributes to the overall scaling of the current.

Material availability

All materials generated during this study including mutant channels are available upon request.

Data availability

All data generated or analyzed during this study are included in the manuscript and supporting files. The source code for simulations is provided in supplementary information.

Acknowledgements

Additional information

Competing interests

Marcel P Goldschen-Ohm: Reviewing editor, *eLife*. The other authors declare that no competing interests exist.

Author contributions

Bochuan Teng, Conceptualization, Data curation, Formal analysis, Investigation, Visualization, Methodology, Writing – original draft, Writing – review and editing; Joshua P Kaplan, Conceptualization, Data curation, Formal analysis, Investigation, Writing – original draft, Writing – review and editing; Ziyu Liang, Formal analysis, Investigation; Kevin Saejin Chyung, Investigation; Marcel P Goldschen-Ohm, Conceptualization, Software, Formal analysis, Funding acquisition, Investigation, Writing – original draft, Writing – review and editing; Emily R Liman, Conceptualization, Resources, Formal analysis, Supervision, Funding acquisition, Visualization, Methodology, Writing – original draft, Project administration, Writing – review and editing

Author ORCIDs

Bochuan Teng http://orcid.org/0000-0001-7918-484X
Joshua P Kaplan http://orcid.org/0000-0001-5064-2130
Marcel P Goldschen-Ohm http://orcid.org/0000-0003-1466-9808
Emily R Liman http://orcid.org/0000-0003-4765-5496

Decision letter and Author response

Decision letter https://doi.org/10.7554/eLife.85317.sa1
Author response https://doi.org/10.7554/eLife.85317.sa2

Additional files

Supplementary files

- Transparent reporting form
- Source code 1. MATLAB scripts for running the kinetic model simulations shown in *Figure 10*.

Data availability

All data generated or analysed during this study are included in the manuscript and supporting files.

References

Baconguis I, Bohlen CJ, Goehring A, Julius D, Gouaux E. 2014. X-Ray structure of acid-sensing ion channel 1-snake toxin complex reveals open state of a Na (+) -selective channel. *Cell* **156**:717–729. DOI: https://doi.org/10.1016/j.cell.2014.01.011, PMID: 24507937

Banerjee A, Lee A, Campbell E, Mackinnon R. 2013. Structure of a pore-blocking toxin in complex with a eukaryotic voltage-dependent K (+) channel. *eLife* **2**:e00594. DOI: https://doi.org/10.7554/eLife.00594, PMID: 23705070

Bohlen CJ, Priel A, Zhou S, King D, Siemens J, Julius D. 2010. A bivalent tarantula toxin activates the capsaicin receptor, TRPV1, by targeting the outer pore domain. *Cell* **141**:834–845. DOI: https://doi.org/10.1016/j.cell.2010.03.052, PMID: 20510930

Bushman JD, Ye W, Liman ER. 2015. A proton current associated with sour taste: distribution and functional properties. *FASEB Journal* **29**:3014–3026. DOI: https://doi.org/10.1096/fj.14-265694, PMID: 25857556

Catterall WA, Cestèle S, Yarov-Yarovoy V, Yu FH, Konoki K, Scheuer T. 2007. Voltage-Gated ion channels and gating modifier toxins. *Toxicon* **49**:124–141. DOI: https://doi.org/10.1016/j.toxicon.2006.09.022, PMID: 17239913

Chang RB, Waters H, Liman ER. 2010. A proton current drives action potentials in genetically identified sour taste cells. *PNAS* **107**:22320–22325. DOI: https://doi.org/10.1073/pnas.1013664107, PMID: 21098668

Chang WW, Matt AS, Schewe M, Musinszki M, Grüssel S, Brandenburg J, Garfield D, Bleich M, Baukrowitz T, Hu MY. 2021. An otopetrin family proton channel promotes cellular acid efflux critical for biomineralization in a marine calcifier. *PNAS* **118**:e2101378118. DOI: https://doi.org/10.1073/pnas.2101378118, PMID: 34301868

Chen Q, Zeng W, She J, Bai XC, Jiang Y. 2019. Structural and functional characterization of an Otopetrin family proton channel. *eLife* **8**:e46710. DOI: https://doi.org/10.7554/eLife.46710, PMID: 30973323

Chu XP, Wemmie JA, Wang WZ, Zhu XM, Saugstad JA, Price MP, Simon RP, Xiong ZG. 2004. Subunit-Dependent high-affinity zinc inhibition of acid-sensing ion channels. *The Journal of Neuroscience* **24**:8678–8689. DOI: https://doi.org/10.1523/JNEUROSCI.2844-04.2004, PMID: 15470133

Colquhoun D, Hawkes AG. 1995. Desensitization of N-methyl-D-aspartate receptors: a problem of interpretation. *PNAS* **92**:10327–10329. DOI: https://doi.org/10.1073/pnas.92.22.10327, PMID: 7479777

Decoursey TE. 2003. Voltage-Gated proton channels and other proton transfer pathways. *Physiological Reviews* **83**:475–579. DOI: https://doi.org/10.1152/physrev.00028.2002, PMID: 12663866

Ganguly A, Chandel A, Turner H, Wang S, Liman ER, Montell C. 2021. Requirement for an otopetrin-like protein for acid taste in *Drosophila*. *PNAS* **118**:e2110641118. DOI: https://doi.org/10.1073/pnas.2110641118, PMID: 34911758

Gilly WF, Armstrong CM. 1982. Divalent cations and the activation kinetics of potassium channels in squid giant axons. *The Journal of General Physiology* **79**:965–996. DOI: https://doi.org/10.1085/jgp.79.6.965, PMID: 6286846

Goldschen-Ohm MP, Chanda B. 2014. Probing gating mechanisms of sodium channels using pore blockers. Goldschen-Ohm MP (Ed). *Handbook of Experimental Pharmacology* Springer. p. 183–201. DOI: https://doi.org/10.1007/978-3-642-41588-3_9, PMID: 24737237

Goldschen-Ohm MP, Haroldson A, Jones MV, Pearce RA. 2014. A nonequilibrium binary elements-based kinetic model for benzodiazepine regulation of GABAA receptors. *The Journal of General Physiology* **144**:27–39. DOI: https://doi.org/10.1085/jgp.201411183, PMID: 24981228

Gordon SE, Zagotta WN. 1995a . A histidine residue associated with the gate of the cyclic nucleotide-activated channels in rod photoreceptors. *Neuron* **14**:177–183. DOI: https://doi.org/10.1016/0896-6273(95)90252-x, PMID: 7530019

Gordon SE, Zagotta WN. 1995b . Subunit interactions in coordination of Ni2+ in cyclic nucleotide-gated channels. *PNAS* **92**:10222–10226. DOI: https://doi.org/10.1073/pnas.92.22.10222, PMID: 7479756

Hille B. 2001. Ionic Channels of Excitable Membranes. Sinauer Associates Inc.

Hu H, Bandell M, Petrus MJ, Zhu MX, Patapoutian A. 2009. Zinc activates damage-sensing TRPA1 ion channels. *Nature Chemical Biology* **5**:183–190. DOI: https://doi.org/10.1038/nchembio.146, PMID: http://www.ncbi.nlm.nih.gov/entrez/query.fcgi?cmd

Hughes I, Blasiole B, Huss D, Warchol ME, Rath NP, Hurle B, Ignatova E, Dickman JD, Thalmann R, Levenson R, Ornitz DM. 2004. Otopetrin 1 is required for otolith formation in the zebrafish *Danio rerio*. *Developmental Biology* **276**:391–402. DOI: https://doi.org/10.1016/j.ydbio.2004.09.001, PMID: 15581873

Hughes I, Binkley J, Hurle B, Green ED, Sidow A, Ornitz DM, NISC Comparative Sequencing Program. 2008. Identification of the otopetrin domain, a conserved domain in vertebrate otopetrins and invertebrate otopetrin-like family members. *BMC Evolutionary Biology* **8**:41. DOI: https://doi.org/10.1186/1471-2148-8-41, PMID: 18254951

Hurle B, Ignatova E, Massironi SM, Mashimo T, Rios X, Thalmann I, Thalmann R, Ornitz DM. 2003. Non-syndromic vestibular disorder with otoconial agenesis in tilted/mergulhador mice caused by mutations in otopetrin 1. *Human Molecular Genetics* **12**:777–789. DOI: https://doi.org/10.1093/hmg/ddg087, PMID: 12651873

Hurle B, Marques-Bonet T, Antonacci F, Hughes I, Ryan JF, Program NCS, Eichler EE, Ornitz DM, Green ED. 2011. Lineage-specific evolution of the vertebrate otopetrin gene family revealed by comparative genomic analyses. *BMC Evolutionary Biology* **11**:23. DOI: https://doi.org/10.1186/1471-2148-11-23, PMID: 21261979

Jumper J, Evans R, Pritzel A, Green T, Figurnov M, Ronneberger O, Tunyasuvunakool K, Bates R, Žídek A, Potapenko A, Bridgland A, Meyer C, Kohl SAA, Ballard AJ, Cowie A, Romera-Paredes B, Nikolov S, Jain R, Adler J, Back T, et al. 2021. Highly accurate protein structure prediction with alphafold. *Nature* **596**:583–589. DOI: https://doi.org/10.1038/s41586-021-03819-2, PMID: 34265844

Karpen JW, Brown RL, Stryer L, Baylor DA. 1993. Interactions between divalent cations and the gating machinery of cyclic GMP-activated channels in salamander retinal rods. *The Journal of General Physiology* **101**:1–25. DOI: https://doi.org/10.1085/jgp.101.1.1, PMID: 7679715

MacKinnon R, Heginbotham L, Abramson T. 1990. Mapping the receptor site for charybdotoxin, a pore-blocking potassium channel inhibitor. *Neuron* **5**:767–771. DOI: https://doi.org/10.1016/0896-6273(90)90335-d, PMID: 1702643

Mathie A, Sutton GL, Clarke CE, Veale EL. 2006. Zinc and copper: pharmacological probes and endogenous modulators of neuronal excitability. *Pharmacology & Therapeutics* **111**:567–583. DOI: https://doi.org/10.1016/j.pharmthera.2005.11.004, PMID: 16410023

Mi T, Mack JO, Lee CM, Zhang YV. 2021. Molecular and cellular basis of acid taste sensation in *Drosophila*. *Nature Communications* **12**:3730. DOI: https://doi.org/10.1038/s41467-021-23490-5, PMID: 34140480

Noh S, Lee SR, Jeong YJ, Ko KS, Rhee BD, Kim N, Han J. 2015. The direct modulatory activity of zinc toward ion channels. *Integrative Medicine Research* **4**:142–146. DOI: https://doi.org/10.1016/j.imr.2015.07.004, PMID: 28664120

Parikh K, Antanaviciute A, Fawkner-Corbett D, Jagielowicz M, Aulicino A, Lagerholm C, Davis S, Kinchen J, Chen HH, Alham NK, Ashley N, Johnson E, Hublitz P, Bao L, Lukomska J, Andev RS, Björklund E, Kessler BM,

Fischer R, Goldin R, et al. 2019. Colonic epithelial cell diversity in health and inflammatory bowel disease. *Nature* **567**:49–55. DOI: https://doi.org/10.1038/s41586-019-0992-y, PMID: 30814735

Peralta FA, Huidobro-Toro JP. 2016. Zinc as allosteric ion channel modulator: ionotropic receptors as metalloproteins. *International Journal of Molecular Sciences* **17**:1059. DOI: https://doi.org/10.3390/ijms17071059, PMID: 27384555

Ramsey IS, Moran MM, Chong JA, Clapham DE. 2006. A voltage-gated proton-selective channel lacking the pore domain. *Nature* **440**:1213–1216. DOI: https://doi.org/10.1038/nature04700, PMID: 16554753

Rulíšek L, Vondrášek J. 1998. Coordination geometries of selected transition metal ions (co2+, ni2+, cu2+, zn2+, cd2+, and hg2+) in metalloproteins. *Journal of Inorganic Biochemistry* **71**:115–127. DOI: https://doi.org/10.1016/s0162-0134(98)10042-9, PMID: 9833317

Sack JT, Aldrich RW. 2006. Binding of a gating modifier toxin induces intersubunit cooperativity early in the shaker K channel's activation pathway. *The Journal of General Physiology* **128**:119–132. DOI: https://doi.org/10.1085/jgp.200609492, PMID: 16801385

Saotome K, Teng B, Tsui CCA, Lee WH, Tu YH, Kaplan JP, Sansom MSP, Liman ER, Ward AB. 2019. Structures of the otopetrin proton channels otop1 and otop3. *Nature Structural & Molecular Biology* **26**:518–525. DOI: https://doi.org/10.1038/s41594-019-0235-9, PMID: 31160780

Shcheglovitov A, Vitko I, Lazarenko RM, Orestes P, Todorovic SM, Perez-Reyes E. 2012. Molecular and biophysical basis of glutamate and trace metal modulation of voltage-gated Ca (V) 2.3 calcium channels. *The Journal of General Physiology* **139**:219–234. DOI: https://doi.org/10.1085/jgp.201110699, PMID: 22371363

Swartz KJ, MacKinnon R. 1997. Hanatoxin modifies the gating of a voltage-dependent K+ channel through multiple binding sites. *Neuron* **18**:665–673. DOI: https://doi.org/10.1016/s0896-6273(00)80306-2, PMID: 9136774

Teng B, Wilson CE, Tu YH, Joshi NR, Kinnamon SC, Liman ER. 2019. Cellular and neural responses to sour stimuli require the proton channel otop1. *Current Biology* **29**:3647–3656. DOI: https://doi.org/10.1016/j.cub.2019.08.077, PMID: 31543453

Teng B, Kaplan JP, Liang Z, Krieger Z, Tu YH, Burendei B, Ward AB, Liman ER. 2022. Structural motifs for subtype-specific pH-sensitive gating of vertebrate Otopetrin proton channels. *eLife* **11**:e77946. DOI: https://doi.org/10.7554/eLife.77946, PMID: 35920807

Tian L, Zhang H, Yang S, Luo A, Kamau PM, Hu J, Luo L, Lai R. 2023. Vertebrate OTOP1 is also an alkali-activated channel. *Nature Communications* **14**:26. DOI: https://doi.org/10.1038/s41467-022-35754-9, PMID: 36596786

Trattnig SM, Gasiorek A, Deeb TZ, Ortiz EJC, Moss SJ, Jensen AA, Davies PA. 2016. Copper and protons directly activate the zinc-activated channel. *Biochemical Pharmacology* **103**:109–117. DOI: https://doi.org/10.1016/j.bcp.2016.02.004, PMID: 26872532

Tu YH, Cooper AJ, Teng B, Chang RB, Artiga DJ, Turner HN, Mulhall EM, Ye W, Smith AD, Liman ER. 2018. An evolutionarily conserved gene family encodes proton-selective ion channels. *Science* **359**:1047–1050. DOI: https://doi.org/10.1126/science.aao3264, PMID: 29371428

Vallee BL, Auld DS. 1990. Zinc coordination, function, and structure of zinc enzymes and other proteins. *Biochemistry* **29**:5647–5659. DOI: https://doi.org/10.1021/bi00476a001, PMID: http://www.ncbi.nlm.nih.gov/entrez/query.fcgi?cmd

Vallee BL, Falchuk KH. 1993. The biochemical basis of zinc physiology. *Physiological Reviews* **73**:79–118. DOI: https://doi.org/10.1152/physrev.1993.73.1.79, PMID: 8419966

Varadi M, Anyango S, Deshpande M, Nair S, Natassia C, Yordanova G, Yuan D, Stroe O, Wood G, Laydon A, Žídek A, Green T, Tunyasuvunakool K, Petersen S, Jumper J, Clancy E, Green R, Vora A, Lutfi M, Figurnov M, et al. 2022. AlphaFold protein structure database: massively expanding the structural coverage of protein-sequence space with high-accuracy models. *Nucleic Acids Research* **50**:D439–D444. DOI: https://doi.org/10.1093/nar/gkab1061, PMID: 34791371

Yang H, Liu H, Lin HC, Gan D, Jin W, Cui C, Yan Y, Qian Y, Han C, Wang Z. 2019. Association of a novel seven-gene expression signature with the disease prognosis in colon cancer patients. *Aging* **11**:8710–8727. DOI: https://doi.org/10.18632/aging.102365, PMID: 31612869

Yellen G, Jurman ME, Abramson T, MacKinnon R. 1991. Mutations affecting internal tea blockade identify the probable pore-forming region of a K+ channel. *Science* **251**:939–942. DOI: https://doi.org/10.1126/science.2000494, PMID: 2000494

Zhang X, Bursulaya B, Lee CC, Chen B, Pivaroff K, Jegla T. 2009. Divalent cations slow activation of eag family K+ channels through direct binding to S4. *Biophysical Journal* **97**:110–120. DOI: https://doi.org/10.1016/j.bpj.2009.04.032, PMID: 19580749

Zhang J, Jin H, Zhang W, Ding C, O'Keeffe S, Ye M, Zuker CS. 2019. Sour sensing from the tongue to the brain. *Cell* **179**:392–402. DOI: https://doi.org/10.1016/j.cell.2019.08.031, PMID: 31543264